ORNL/TM-2019/1136

First Annual Progress Report on the Procurement and Post-Irradiation Examination of the Selected Samples of Alloy 800H and Grade 92 and 91 Steels

Lizhen Tan
Tianyi Chen
Kory Linton
Oak Ridge National Laboratory

Collin J. Knight
Idaho National Laboratory

Tarik A. Saleh
Los Alamos National Laboratory

February 28, 2019

OAK RIDGE NATIONAL LABORATORY
MANAGED BY UT-BATTELLE FOR THE US DEPARTMENT OF ENERGY

ORNL/TM-2019/1136
M2NA-17OR0204014

FY 2017 Consolidated Innovative Nuclear Research (CINR)
Nuclear Science User Facilities (NSUF)
Light Water Reactor Sustainability (LWRS)

FIRST ANNUAL PROGRESS REPORT ON THE PROCUREMENT AND POST-IRRADIATION EXAMINATION OF THE SELECTED SAMPLES OF ALLOY 800H AND GRADE 92 AND 91 STEELS

Lizhen Tan, Tianyi Chen, and Kory Linton
Oak Ridge National Laboratory

Collin Knight
Idaho National Laboratory

Tarik Saleh
Los Alamos National Laboratory

Date Published: February 28, 2019

Prepared by
OAK RIDGE NATIONAL LABORATORY
Oak Ridge, TN 37831-6283
managed by
UT-BATTELLE, LLC
for the
US DEPARTMENT OF ENERGY
under contract DE-AC05-00OR22725

CONTENTS

LIST OF TABLES v
LIST OF FIGURES v
ACKNOWLEDGMENTS vii
EXCUTIVE SUMMARY ix
1. INTRODUCTION 1
2. SAMPLE PROCUREMENT 2
2.1 SELECTED INL SAMPLES 2
2.1.1 Reception of The INL Samples at ORNL 3
2.2 SELECTED LANL SAMPLES 3
2.2.1 Reception of The LANL Samples at ORNL 5
2.3 SELECTED ORNL SAMPLES 5
2.3.1 Reception of The ORNL Samples 5
2.4 IRRADIATION CONDITIONS OF THE SELECTED SAMPLES 6
3. TENSILE TEST RESULTS OF THE ORNL SAMPLES 8
3.1 G92-2B SAMPLES 8
3.2 800H/800H-TMP SAMPLES 9
4. HARDNESS TEST RESULTS OF THE ORNL SAMPLES 10
4.1 VICKERS HARDNESS 10
4.2 NANOINDENTATION 11
5. MICROSTRUCTURAL CHARACTERIZATION OF THE ORNL SAMPLES 12
5.1 FRACTOGRAPHY 12
5.2 IRRADIATED MICROSTRUCTURES 12
5.2.1 GB04 (7.44 dpa at ~490°C) 12
5.2.2 GB05 (14.66 dpa at 496.7°C) 13
5.2.3 GB12 (14.63 dpa at ~720°C) 15
6. SUMMARY 16
REFERENCE 17

LIST OF TABLES

Table 1. Selected INL samples. 2
Table 2. Compositions in weight percent (wt%) of the INL samples, with Fe as balance*. 3
Table 3. Selected LANL samples. 4
Table 4. Compositions in weight percent (wt%) of the LANL samples, with Fe as balance. 4
Table 5. Selected ORNL samples. 5
Table 6. Compositions in weight percent (wt%) of the ORNL samples, with Fe as balance. 5
Table 7. Tensile test results of 800H/800H-TMP samples*. 9

LIST OF FIGURES

Figure 1. Irradiation temperature as a function of dose of steel samples irradiated with the G92-2b samples. 6
Figure 2. Irradiation temperature and dose conditions of the selected Grade 92, T91, 800H, and 800H-TMP samples. 7
Figure 3. Stress-strain tensile curves of the selected G92-2b samples tested at room temperature. 8
Figure 4. Dose-dependent (a) yield and tensile strength and (b) uniform and total plastic elongation of the selected G92-2b samples tested at room temperature. 9
Figure 5. Optical images of representative indents on GB04, GB05, and GB12 illustrate the morphologies of the indents, which are not in the same scale bar. 10
Figure 6. Stress-strain tensile curves of the selected G92-2b samples tested at room temperature. 11
Figure 7. Fractography of the tensile-tested GB04, GB05, and GB12 samples. 12
Figure 8. BF (a, d) STEM and (b-c) TEM images of GB04 showing its (a) overview, (b-c) precipitates, and (d) dislocations at the tab section of the tensile specimen. 13
Figure 9. BF STEM images of GB04 at the (a-b) gauge and (c) fracture surface. 13
Figure 10. BF (a-b) STEM and (c-e) images and corresponding FFTs of (d-e) of GB05 at the tab section. 14
Figure 11. BF (a-b) STEM and (c) TEM images of GB05 at the gauge section. 14
Figure 12. BF (a-b) STEM and (c-e) images and corresponding FFTs of (d-e) of GB12 at the tab section. 15
Figure 13. BF STEM images of GB12 at the (a-b) gauge and (c) fracture surface. 15

ACKNOWLEDGMENTS

This research was sponsored by the U.S. Department of Energy (DOE), Office of Nuclear Energy (NE), the FY 2017 Consolidated Innovative Nuclear Research (CINR) Nuclear Science User Facilities (NSUF) program and the Light Water Reactor Sustainability (LWRS) program. We gratefully acknowledge the support provided by Alison Hahn of DOE-NE and Rory Kennedy of Idaho National Laboratory for the NSUF access support and Keith Leonard of Oak Ridge National Laboratory (ORNL) for the research and development support under the LWRS program.

The authors are grateful to Kurt Terrani, NSUF technical leader of ORNL, for supporting this project and Alicia Raftery, Ben Garrison, Clay Morris, Mark Delph, Patricia Tedder, and Joshua Schmidlin of ORNL for sample sorting and reception. Kevin Field and Xiang Chen of ORNL are appreciated for technical review of this report.

EXCUTIVE SUMMARY

Ferritic-martensitic steel Grade 92, with Grade 91 as a reference, together with austenitic stainless steel (or Incoloy Alloy) 800H and its grain-boundary-engineered version 800H-TMP (Thermo-Mechanical Processing), is investigated in this project. A total of fifteen Grade 92 samples from two or three heats, four T91 samples from two heats, and six 800H and six 800H-TMP samples from one heat were selected, which were primarily irradiated in the Advanced Test Reactor (ATR) of Idaho National Laboratory (INL), with the rest in the High Flux Isotope Reactor (HFIR) of Oak Ridge National Laboratory (ORNL), BOR-60 of Russia, and Phénix reactor of France. The samples were irradiated in the temperature range of 241 to 720°C and a dose range of 1.28 to ~70 displacements per atom. All the INL and ORNL samples and part of the LANL (Los Alamos National Laboratory) samples have been received at the Irradiated Materials Examination and Testing (IMET) hot cell facility.

The selected ORNL samples include six Grade 92 and two 800H samples, which were irradiated in the HFIR to 0.46–14.66 dpa at 400 to ~720°C. The Grade 92 is an optimized heat and named as G92-2b. The two 800H samples have one sample as the standard solution-annealed condition and the other sample as a TMP condition with a maximized fraction of low-Σ coincidence site lattice (CSL) boundaries. Tensile test of the G92-2b samples were conducted at room temperature in the IMET hot cell. The lower temperature irradiation at 400–496.7°C to 0.52–14.66 dpa resulted in minimal changes in tensile properties. However, the higher temperature irradiation at ~683.3–720°C to 0.46–14.63 dpa tended to reduce yield and tensile strength by about –136 to –311 MPa and plastic elongation by –1 to –3% with the increasing dose. The 800H and 800H-TMP samples were tensile-tested at their irradiation temperature 580°C in the IMET hot cell, which showed >40% increase in yield and tensile strength with nearly 9% reduction in elongation for 800H-TMP compared with 800H.

Three of the G92-2b samples, i.e., GB04 (7.44 dpa at ~490°C), GB05 (14.66 dpa at 496.7°C), and GB12 (14.63 dpa at ~720°C), were examined at the LAMDA for Vickers hardness measurements and microstructural characterization by SEM and TEM. Vickers hardness was successfully measured on GB12, which was reduced by is – (112.4 ± 12.3) HV1 from the control sample. However, the Vickers hardness measurements were failed on GB04 and GB05 because the samples were polished too thin to prevent the interference from the substrate (epoxy). The other half of the GB04 and GB05 will be polished for the hardness measurements, as well as nanoindentation studies.

Fractography by SEM indicated increased numbers of ductile dimples (or voids) with the increasing irradiation dose, while significantly increased numbers and sizes of dimples with the increasing irradiation temperature. TEM characterization exhibited the presence of $Cr_{23}C_6$, VN, and Laves precipitates at boundaries and matrix, which showed pronounced precipitate-dislocation interactions (pinning effect). Dense dislocations but limited dislocation loops were observed in the samples, which noticeably reduced in GB12. Additionally, some tiny partially amorphized spherical domains were observed in GB12, which had a normal body-centered cubic lattice parameter of 9Cr steels at the surround regions but ~11% smaller than the lattice parameter of the matrix away from the amorphized spherical domains. Further characterization will be pursued to clarify the new findings.

1. INTRODUCTION

Advanced alloys are desired to provide greater safety margins, design flexibility and economics compared to traditional reactor materials. Grade 92 ferritic-martensitic steel and austenitic Alloy 800/800H are two of the promising alloys interested by the current Advanced Radiation-Resistant Materials (ARRM) and Light Water Reactor Sustainability (LWRS) programs. However, systematic studies on neutron-irradiation induced changes in microstructures and mechanical properties are deficient for the alloys. The objective of this project is to develop correlations between microstructures and mechanical properties of the neutron-irradiated Grade 92 and Alloy 800/800H, based on the experimental results generated from this work. It is expected to develop broader correlations for these types of steels by comparing the results of this work with that of similar alloys such as Grade 91, Alloy 709 and type 304/316 stainless steels from literature and the ongoing studies, with the aid of thermodynamics, kinetics, and microstructural hardening modeling.

Samples of Grade 92 and Alloy 800H selected in this work were primarily irradiated in two test reactors for up to ~14 displacements per atom (dpa) at ~241–720°C. Samples of Grade 91, irradiated in the same reactors, were selected as references of Grade 92. Few samples from other two reactors will be included for comparison. Both irradiated and unirradiated samples from the same heat of the materials will be examined to elucidate the radiation-induced evolutions in microstructures, mechanical properties, and deformation mechanisms. To be more specific, mechanical properties such as tensile properties, modulus, hardness, and viscoplasticity will be measured through tensile, Vickers hardness and nanoindentation tests. Microstructural characterization of the samples will be carried out using the state-of-the-art instruments and techniques provided through the Nuclear Science User Facilities (NSUF). The obtained experimental results will then be used to establish the knowledgebase on the effects of alloy chemistry, thermomechanical-processing, and irradiation conditions on microstructures and mechanical properties of Grade 92 and Alloy 800H.

Outcomes of this project will include a comprehensive set of data including microstructures and mechanical properties of both irradiated and unirradiated samples of the interested steels, which will not only help understanding the essential performance of similar alloys, but more importantly to gain indispensable insights into the development of advanced alloys with superior radiation resistance. The outcomes can also serve as inputs and/or benchmarks for microstructural and mechanical property modeling of irradiated ferritic-martensitic and austenitic steels. The accomplishment of this project will directly benefit the LWRS program and bring values to the Advanced Reactor Technologies and Small Modular Reactors programs.

Procurement of the interested neutron-irradiated samples is a critical step to accomplish the goal of this project. This report summarizes the identification and shipment progress for the interested samples at Idaho National Laboratory (INL), Los Alamos National Laboratory (LANL), and Oak Ridge National Laboratory (ORNL), which are to be received and examined at ORNL for this project. The selected ORNL samples were irradiated in the High Flux Isotope Reactor (HFIR) of ORNL, which have been tensile-tested in hot cell of ORNL and part of the samples have been examined. This report summarizes the post-irradiation examination progress of the ORNL samples.

2. SAMPLE PROCUREMENT

2.1 SELECTED INL SAMPLES

A total of twelve INL samples of steels 800H, NF616, and T91 were selected, which were irradiated in the Advanced Test Reactor (ATR) of INL through the University of Wisconsin Pilot Project of the ATR National Scientific User Facility [1]. The steels 800H, NF616, and T91 were commercial heats distributed by INL, Japan Atomic Energy Agency (JAEA), and INL, respectively. The selected samples are listed in Table 1. The samples are in two types, with one type as type SS-J2 miniature specimens and the other type as 3-mm diameter discs.

Table 1. Selected INL samples.

Specimen type	Alloy	Engraved sample code	KGT Num	Temperature (°C)		Dose (dpa)		Dose rate (dpa/s)
				Planned	Average as-run	Planned	As-run total	
Type SS-J2 miniature tensile specimen with 16 × 4 × (<1) mm and gauge 5 × 1.2 × (<1) mm.	800H	N4	1712	400	359	6	7.27	1.30×10^{-7}
		N5	1772	500	451.5	3	3.9	1.35×10^{-7}
		N6	1806	500	431	6	9.01	1.61×10^{-7}
	800H-TMP	P4	2578	400	359	6	7.36	1.31×10^{-7}
		P5	2596	500	451.5	3	3.95	1.37×10^{-7}
		P6	2597	500	431	6	9.12	1.63×10^{-7}
	NF616	D1*	402	300	241	3	3.51	1.29×10^{-7}
		D2	1791	300	291.5	6	2.96	5.29×10^{-8}
		D4	1735	400	359	6	5.91	1.06×10^{-7}
		D6	1783	500	431	6	8.16	1.46×10^{-7}
3-mm diameter disc (~0.2-mm thick)	T91	A4	1729	400	447.5	6	4.78	8.51×10^{-8}
		A6	1790	500	429.5	6	7.79	1.39×10^{-7}

* The sample D1 is at Argonne National Laboratory (ANL), which is to be in-situ tensile-tested during high-energy x-ray diffraction using the Advanced Photon Source (APS) of ANL.

Other than the standard solution-annealed condition (1177°C for 24 minutes per centimeter of thickness, followed by a water quench) of austenitic stainless steel 800H, a thermomechanically processed (TMP) condition, named as 800H-TMP, was irradiated simultaneously. The TMP was constituted of a 6.6 ± 0.2 % thickness reduction by rolling at room temperature, followed by annealing at 1050°C for 90 minutes and water quench, which is a grain boundary engineering (GBE) method to significantly increase the fraction of low-Σ coincidence site lattice (CSL) boundaries, e.g., nearly 70% (800H-TMP) and ~40% (800H) low-Σ CSL boundaries [2]. GBE with a significantly increased fraction of low-Σ CSL boundaries would benefit a variety of properties such as strength and resistance to creep, stress corrosion cracking, and oxidation [3]. The 800H-TMP exhibited noticeable enhancements in the resistance to thermal aging [4] and corrosion in supercritical water and high-temperature air [5,6,7,8]. Preliminary studies also showed more or less improvements in resistance to neutron irradiation [9,10]. Therefore, three samples of 800H-TMP, together with three samples of 800H irradiated in nearly identical conditions, were selected in this project to confirm and elucidate the beneficial effects of GBE/TMP on the neutron irradiation resistance of 800H. The other set of samples are ferritic-martensitic steels NF616 and T91, classic/typical versions of Grade 92 and 91, respectively. T91 samples are to be used as reference for NF616.

Each sample was engraved with a unique sample code for visual sample identification and assigned with a unique KGT number for sample library record. The information, together with the planned and as-run irradiation temperature and dose listed in Table 1, was obtained from the material library presented online

at https://nsuf.inl.gov. The dose rate in Table 1 was deduced from as-run neutron fluence divided by irradiation time. The irradiation conditions, e.g., temperature and dose, will be compared with the analytical reports of the University of Wisconsin Pilot Project [11,12,13].

The compositions in weight percent (wt%) of 800H, NF616, and T91 of the INL samples are listed in Table 2 [1]. The compositions are critical for alloy thermodynamic analysis and transmutation analysis to interpret the experimental observations in this project.

Table 2. Compositions in weight percent (wt%) of the INL samples, with Fe as balance*.

Alloy	Cr	Ni	Mn	Si	Ti	Al	V	W	Mo	Nb	Cu	C	N	P	S
800H/ 800-TMP	20.42	31.59	0.76	0.13	0.57	0.50					0.42	0.069		0.014	0.001
NF616	8.82	0.174	0.45	0.102		0.005	0.194	1.87	0.468	0.064		0.109	0.0474	0.012	0.0032
T91	8.37	0.21	0.45	0.28		0.022	0.216		0.90	0.076	0.17	0.1	0.048	0.009	0.003

* The blank cells are the elements not measured or reported. Oxygen and boron contents were reported as 0.0042% and 0.0017%, respectively, in NF616, which were not reported in the other alloys. 800H was solution-annealed at 1177°C for 24 minutes per centimeter of thickness, followed by a water quench. 800H-TMP was based on 800H, subjected to ~6.6% thickness reduction by rolling at room temperature and then annealed at 1050°C for 1.5 h with water quench. NF616 was normalized at 1070°C for 2 h and tempered at 770°C for 2 h with air cooling. T91 was normalized at 1066°C for 0,8 h and tempered at 790°C for 0.7 h with air cooling.

2.1.1 Reception of the INL Samples at ORNL

One of the NF616 samples, with an engraved sample code of D1, is at ANL, which will be examined by *in-situ* tensile test during high-energy x-ray diffraction using the APS of ANL. The tested D1 will be shipped to ORNL for microstructural characterization and hardness measurements. Therefore, a total of eleven samples, i.e., nine SS-J2 tensile specimens and two 3-mm diameter discs, were shipped from INL to ORNL. ORNL has received the eleven samples in the Irradiated Materials Examination and Testing (IMET) hot cell facility at 3025E. The nine SS-J2 tensile specimens are planned to be tensile-tested at room temperature in next few months right after the completion of instrument updates.

2.2 SELECTED LANL SAMPLES

Three sets of LANL samples were identified, which are classified by their irradiation reactors, i.e., ATR, BOR-60, and Phénix. The samples and their respective conditions are listed in Table 3, together with their alloy compositions listed in Table 4.

Table 3. Selected LANL samples.

Specimen type	Alloy	Sample ID	Temperature (°C)	Dose (dpa)	Irradiation reactor	Comment
Type SS-J2 tensile	T91	TA04	295	6.5	ATR	Tensile-tested at 25°C [14]
		TA#1c [a]		0		
Ø3-mm TEM discs		T108	517	28	BOR-60	Shared with an IRP project
	NF616	N71	425	19.6		
		N64	524	15.4		
		N133	517	28		
Type SS-J3 tensile or Ø3-mm TEM discs	800H	TBI [b]	~400 and ~500 [c]	Up to ~70 [c]	Phénix	The Phénix MATRIX experiment
	800H-TMP					
	NF616					

[a] Unirradiated control sample of the irradiated T91 (i.e., TA04).
[b] TBI – to be identified.
[c] Planned temperatures and dose, unlike the other analyzed temperatures and doses.

Table 4. Compositions in weight percent (wt%) of the LANL samples, with Fe as balance.

Alloy	Cr	Ni	Mn	Si	Ti	Al	V	W	Mo	Nb	Cu	C	N	P	S
T91 *	9.22	0.18	0.46	0.24	0.002	0.009	0.24	0.013	0.96	0.063	0.087	0.052	0.057	0.016	0.001
NF616	The Phénix samples are from the same heat as that in the INL samples; the BOR-60 samples are likely to be the same heat as the INL samples, which is to be confirmed.														
800H/ 800-TMP	The Phénix samples are from the same heat as that in the INL samples.														

* Also reported 0.002O and 0.021Co. The steel was normalized at 1040°C for 1 h with air cooling and tempered at 760°C for 1 h with air cooling [14]. The T91 sample T108 is from the same provider as that of the INL samples, which is likely to be the same heat to be confirmed.

The selected ATR set of samples only have one T91 sample (i.e., TA04 in Table 3) irradiated at ~295°C to ~6.5 dpa, which has the lowest irradiation temperature in all the identified T91 samples. It complements the INL T91 samples listed in Table 1 as a baseline for comparison with NF616. The TA#1c is an unirradiated control sample for TA04. The TA04 and TA#1c samples were tensile-tested at room temperature, with the results reported by Maloy et al. [14].

The selected BOR-60 set of samples have T91 and NF616 samples irradiated to 15.4–28 dpa at 425–524°C, which are shared with an Integrated Research Project (IRP) under the Nuclear Energy University Program (NEUP) of U.S. Department of Energy. The NF616 was from the same source as that in the INL samples. They are likely to be the same heat, which is to be confirmed. The BOR-60 samples also include 800H samples, which had been sufficiently characterized. The results will be included in this project for comparison. The BOR-60 samples are all TEM disc type specimens and thus only provide hardness and microstructure results. There are multiple samples per condition for each alloy. Therefore, the sample ID of the BOR-60 samples characterized in this project may be different from that listed in Table 3.

The selected Phénix set of samples include 800H, 800H-TMP, and NF616 samples irradiated up to ~70 dpa at planned irradiation temperatures of ~400 and ~500°C. The analyzed irradiation temperatures and doses will be available later. The samples are in type SS-J3 miniature tensile specimens (similar to SS-J2 with a thicker thickness) and 3-mm diameter TEM discs, which are from the same heat as that in the INL samples.

2.2.1 Reception of the LANL Samples at ORNL

The ATR and BOR-60 sets of samples are being shipped to ORNL. The Phénix set of samples are expected to be available in early FY 2021, which may only provide some preliminary results for this project because of the timeline.

2.3 SELECTED ORNL SAMPLES

The selected ORNL samples include G92-2b and 800H samples irradiated to 0.46–14.66 dpa at 400 to ~720°C in the HFIR of ORNL, which are listed in Table 5, together with the alloy composition and condition in Table 6. The G92-2b is a heat of optimized Grade 92, which were developed under the Advanced Reactor Technologies (ART) program [15]. It showed improved strength and creep resistance compared with conventional Grade 92 such as NF616. The AR2 and HG1 samples are 800H and 800H-TMP, respectively, from the same heat as the INL samples, as well as the Phénix set of samples, with composition listed in Table 2.

Table 5. Selected ORNL samples.

Specimen type	Alloy	Sample ID	Temperature (°C)	Dose (dpa)
SS-J2	G92-2b	GB03	400	0.52
		GB04	~490	7.44
		GB05	496.7	14.66
		GB10	683.3	0.46
		GB11	~720	7.44
		GB12	~720	14.63
SS-3	800H	AR2	580	1.28
	800H-TMP	HG1		

Table 6. Compositions in weight percent (wt%) of the ORNL samples, with Fe as balance.

Alloy	Cr	Ni	Mn	Si	V	W	Mo	Nb	C	N	B
G92-2b *	8.9	0.10	0.47	0.14	0.23	1.9	0.43	0.11	0.087	0.045	<0.002
800H/ 800-TMP	The same as the INL and Phénix samples.										

* The heat was normalized at 1080°C for 1 h, followed by hot-rolling to 0.6”-thick plate from 1” at 1080°C and water quench, and tempered at 750°C for 2 h with air cooling.

2.3.1 Reception of the ORNL Samples

The selected ORNL samples have been located. Some of the samples have been tensile-tested at the IMET hot cell facility and being examined in the Low Activation Materials Design and Analysis (LAMDA) laboratory of ORNL.

2.4 IRRADIATION CONDITIONS OF THE SELECTED SAMPLES

Ferritic-martensitic steel Grade 92, with T91 as a reference, together with austenitic stainless steel (or Incoloy Alloy) 800H and its GBE-treated version 800H-TMP, is investigated in this project. A total of fifteen Grade 92 samples, four T91 samples, six 800H and six 800H-TMP samples were selected, which were primarily irradiated in the ATR, some in the HFIR, and few in the BOR-60 and Phénix reactors. The selected samples of Grade 92 were from two or three heats, T91 from two heats, and 800H and 800H-TMP from one heat. The irradiation temperatures and doses of the selected samples were primarily obtained from engineering calculations and analysis, together with some support from SiC temperature monitor analysis, of the relevant irradiation experiments.

Figure 1 shows an example of the analyzed irradiation temperatures of the ORNL steel samples, including G92-2b samples, from the available SiC temperature monitor samples in the same irradiation campaign as a function of irradiation dose in a logarithmic scale. Each dose has three temperature data points from three SiC samples at the top, middle, and bottom sections of irradiation capsules, which are not differentiated in the plot. The bottom section had relatively stable temperatures, while the top section had relatively large variations with increasing doses. The middle section generally had the highest temperatures, especially at higher doses. Some of the irradiation temperatures in Table 5 are reported according to the analyzed results of the accompanied SiC temperature monitor samples, while the approximate temperatures with a "~" sign are estimated from extrapolation according to the available SiC temperature monitor results from steel samples (including some G92-2b samples) in the same irradiation experiment as shown in Figure 1.

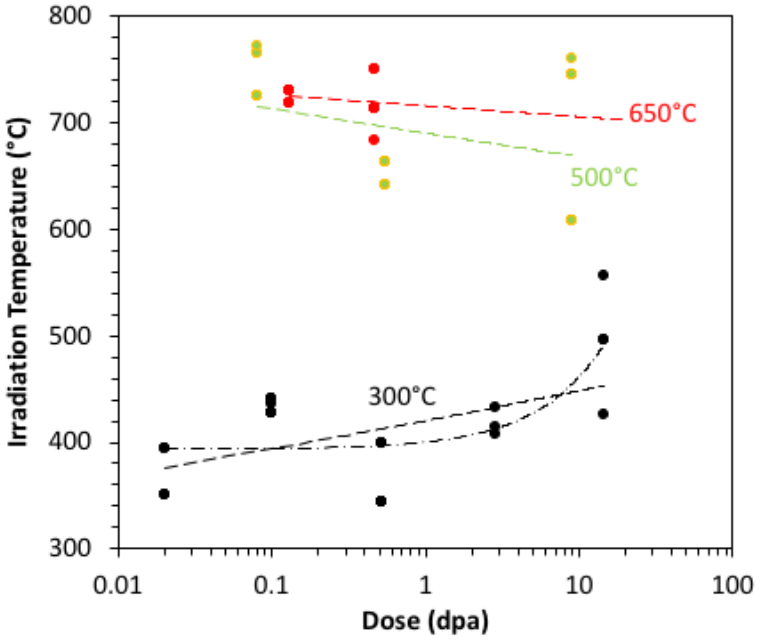

Figure 1. Irradiation temperature as a function of dose of steel samples irradiated with the G92-2b samples.

The dose-dependent irradiation temperature data are roughly fitted with a power function as shown in dashed lines in Figure 1, while the data for the planned 300°C irradiation also exhibited a better fitting by a linear function as shown in a dash-dot line. In general, the planned 300°C irradiation turns out to be above ~350°C and increasing with higher doses, especially for doses above 1 dpa. In contrast, the planned 500 and 650°C irradiations had similar irradiation temperatures, tending to slightly decrease with increasing doses. According to Figure 1, it is expected that GB04 at the middle section of the irradiation capsule was irradiated at ~490°C, while GB11 and GB12 at the middle section of the irradiation capsule was irradiated at ~720°C. The irradiation temperatures of the G92-2b samples were ~100–200°C and ~30–70°C higher

than the planned 300 and 650°C. One of factors causing such large increases from the planned temperatures would be gamma heat generated from tungsten samples that were irradiated with the steel samples in the same capsules. The selected Grade 92 samples irradiated in the Advanced Test Reactor (ATR) of Idaho National laboratory were irradiated at temperatures in the range of 241–431°C, which will provide low-temperature properties to have an overall picture about radiation resistance of Grade 92.

The irradiation temperature and dose conditions of the selected Grade 92, T91, 800H, and 800H-TMP samples are plotted in Figure 2. The Grade 92 samples have a large irradiation condition range, with the T91 samples consistent in a couple of the conditions. The 800H and 800H-TMP samples have excellent consistency in the irradiation conditions.

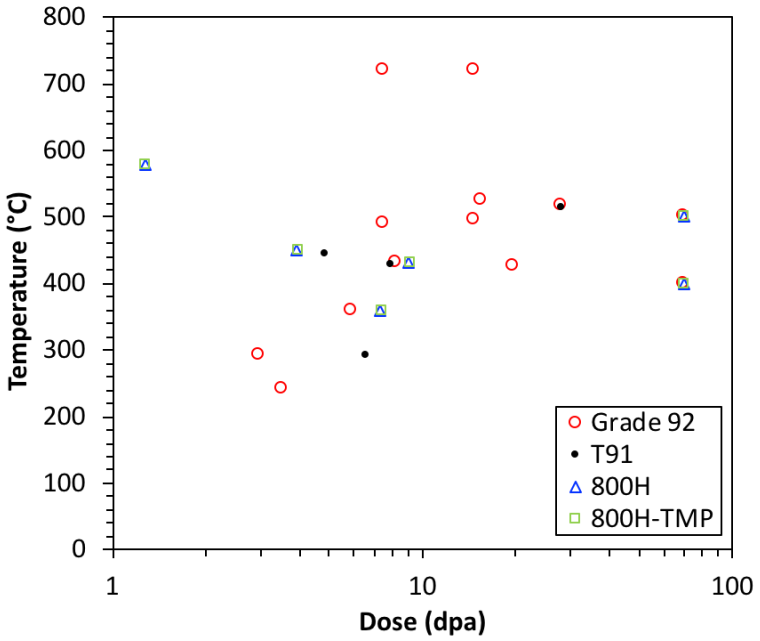

Figure 2. Irradiation temperature and dose conditions of the selected Grade 92, T91, 800H, and 800H-TMP samples.

3. TENSILE TEST RESULTS OF THE ORNL SAMPLES

Tensile test was conducted at room temperature in the IMET hot cell facility, using shoulder load at a strain rate of 0.001/s.

3.1 G92-2B SAMPLES

Figure 3 shows the stress-strain curves of the selected G92-2b samples, together with the same heat unirradiated control sample, tested at room temperature. Part of the tensile testing curves were reported recently [16]. The 400–496.7°C irradiated samples GB03, GB04, and GB05 exhibited elastic modulus comparable to the control sample. However, the higher temperature irradiated samples exhibited noticeable lower elastic modulus. The GB10 (6873.3°C) and GB12 (~720°C) showed comparable elastic modulus, but the GB11 (~720°C) had a much lower elastic modulus. Microstructural characterization of the samples may help clarify the potential causes for the changes.

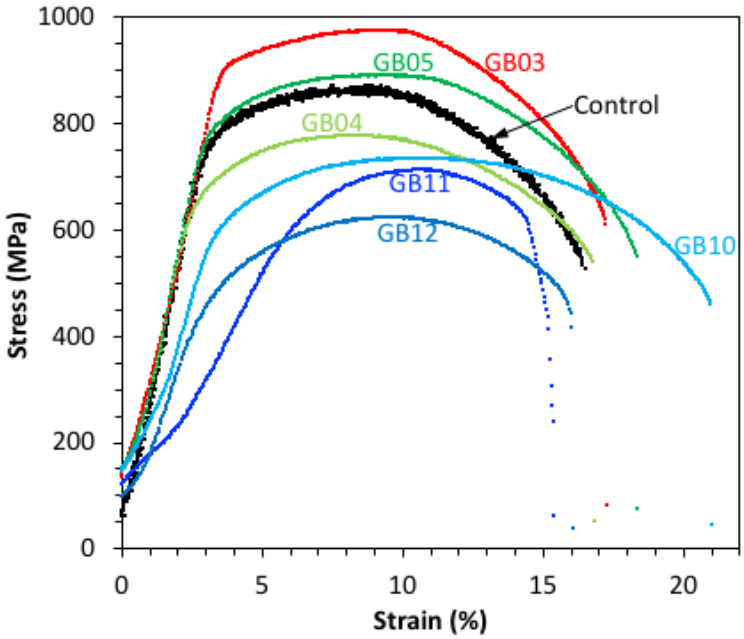

Figure 3. Stress-strain tensile curves of the selected G92-2b samples tested at room temperature.

By analyzing the curves, the tensile properties such as yield and tensile strength and uniform and total plastic elongation were obtained and are plotted in Figure 4 as a function of dose of the samples. The 0.52 dpa irradiation at 400°C resulted in small increases in yield and tensile strength by 115–153 MPa but without noticeable changes in uniform and total plastic elongation. The increased doses to 7.44 and 14.66 dpa at ~490–496.7°C caused small reductions of yield and tensile strength close to that of the control sample, with minimal changes or slight increases in uniform and total plastic elongation. In contrast, the 0.46 and 7.44 dpa irradiation at ~683.3–720°C consistently reduced some yield and tensile strength by about –136 to –168 MPa, with decreasing uniform and total plastic elongation with the increasing dose. The higher dose 14.63 dpa irradiation at ~720°C resulted in further decreases in yield and tensile strength, but without noticeable recovery of uniform and total plastic elongation.

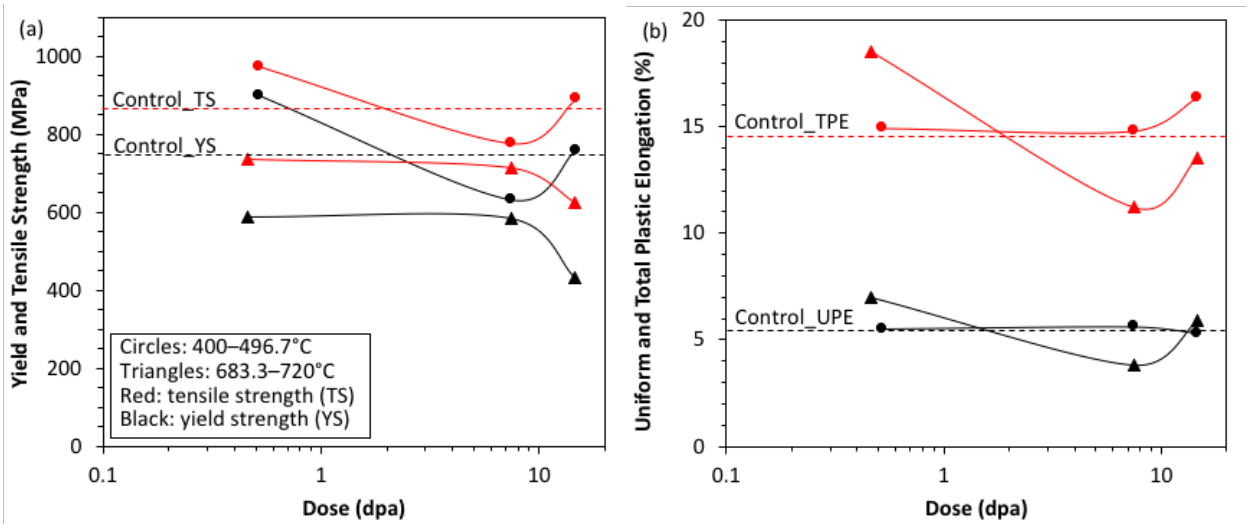

Figure 4. Dose-dependent (a) yield and tensile strength and (b) uniform and total plastic elongation of the selected G92-2b samples tested at room temperature.

3.2 800H/800H-TMP SAMPLES

Tensile testing of the 800H and 800H-TMP samples were tested at room temperature by another program. The tensile properties of the two samples are listed in Table 7, with the results reported by Nanstad et al. [17]. The tensile results tested at the irradiation temperature 580°C indicate noticeable increases in yield and ultimate (or tensile) strength by ~130–150 MPa, with little reductions in uniform and total elongation by about –0.7 to –1.1%. Hardness measurements and microstructural characterization of the two samples have not been performed, which will be pursued to correlate with the tensile properties.

Table 7. Tensile test results of 800H/800H-TMP samples*.

Alloy	Sample	Yield strength (MPa)	Ultimate strength (MPa)	Uniform elongation (%)	Total elongation (%)
800H	AR2	272.0	362.4	8.05	12.9
800H-TMP	HG1	403.7	514.4	7.34	11.8

*The samples were irradiated in HFIR to 1.28 dpa at 580°C, which were tensile-tested at 580°C.

4. HARDNESS TEST RESULTS OF THE ORNL SAMPLES

Only three of the G92-2b samples, i.e., GB04, GB05, and GB12, were received at the LAMDA laboratory of ORNL from the IMET hot cell facility of ORNL. Therefore, only the three samples have been subjected to hardness measurements and microstructural characterization, presented in this and the next Sections.

4.1 VICKERS HARDNESS

The GB04, GB05, and GB12 samples, together with the same heat unirradiated control sample, were mounted in conductive epoxy and mechanically polished to a mirror finish. Vickers microhardness was measured on the polished samples at 0.1, 0.5, and 1 kgf with three or five measurements per condition. The optical images of representative indents are shown in Figure 5, which are not in the same scale bar. In contrast to the normal diamond shape of the Vickers indents on GB12 and that on GB04 at 0.1 kgf, the indents on the GB04 at the other loads and GB05 are in an abnormal star shape.

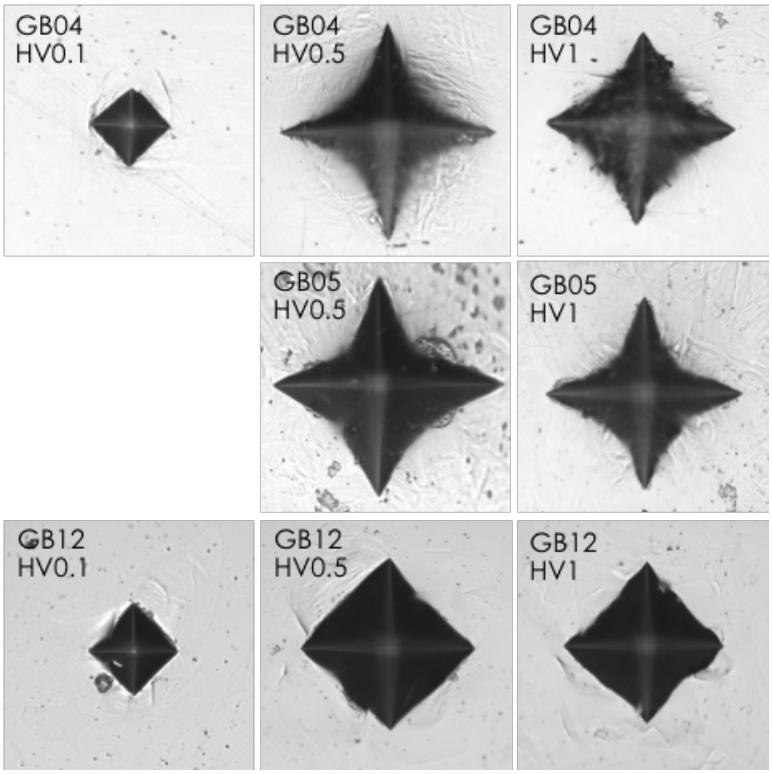

Figure 5. Optical images of representative indents on GB04, GB05, and GB12 illustrate the morphologies of the indents, which are not in the same scale bar.

The Vickers hardness as a function of the indentation depth of GB04, GB05, and GB12, together with the control sample and the epoxy, is plotted in Figure 6. The results of GB12 are normal, showing a small reduction in hardness from 167.6 ± 14.9 HV0.1 to 147.6 ± 11.1 HV1 with the increasing indentation depth (or load), which have small standard deviations roughly comparable to that of the control sample and epoxy. The hardness of GB12 is – (112.4 ± 12.3) HV1 reduced from the control sample. In contrast, the GB04 and GB05 had pronounced reductions in hardness with the increasing indentation depth, which have significant larger standard deviations. The depth-dependent hardness of both GB04 and GB05 is obviously approaching that of the epoxy. Therefore, the results of GB04 and GB05 were greatly influenced by the substrate, i.e., epoxy, because the two samples were polished too thin to have representative bulk hardness

property of the samples, consequently resulting in the star shape indents on GB04 and GB05 as shown in Figure 5.

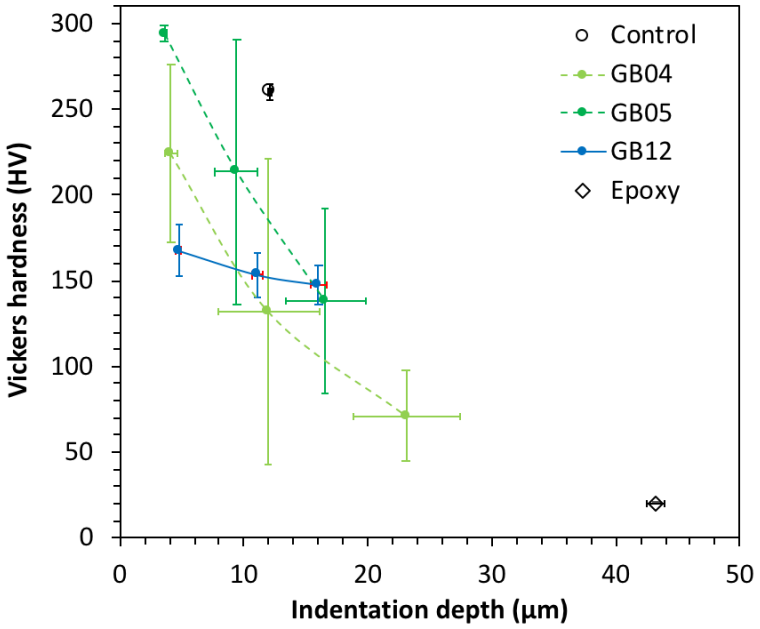

Figure 6. Stress-strain tensile curves of the selected G92-2b samples tested at room temperature.

4.2 NANOINDENTATION

Nanoindentation using Keysight Technologies Nano Indenter G200 was practiced on GB04 and GB05, using the continuous stiffness measurement technique with a maximum of 1 µm indentation depth. The obtained Young's moduli were abnormally low as 159 ± 20 and 116 ± 35 GPa, respectively, for the two samples. It indicates that such a lower level of load (or indentation depth) under nanoindentation was still influenced by the substrate epoxy as indicated by the Vickers hardness measurements. Therefore, the other part of the tensile-fractured sample of GB04 and GB05 is being requested for polishing and Vickers and nanoindentation studies, to be compared with the other selected samples and control sample.

5. MICROSTRUCTURAL CHARACTERIZATION OF THE ORNL SAMPLES

Microstructural characterization of the samples was primarily performed using scanning electron microscopy (SEM) and transmission electron microscopy (TEM).

5.1 FRACTOGRAPHY

Figure 7 shows fractography of the three received samples, i.e., GB04, GB05, and GB12, at LAMDA using SEM in a secondary electron imaging mode. Noticeably greater necking was observed for the ~490–496.7°C irradiated GB04 and GB05 compared with the ~720°C irradiated GB12, which is consistent with the tensile curves in Figure 3, showing a smaller difference between the total and uniform elongation of GB12 compared with GB04 and GB05. The higher irradiation dose of GB05 (14.66 dpa) increased ductile dimples (or voids) primarily in number density compared with GB04 (7.44 dpa). However, the higher irradiation temperature of GB12 (~720°C) significantly increased dimples in both density and size compared with GB05 (496.7°C) irradiated to about the same dose.

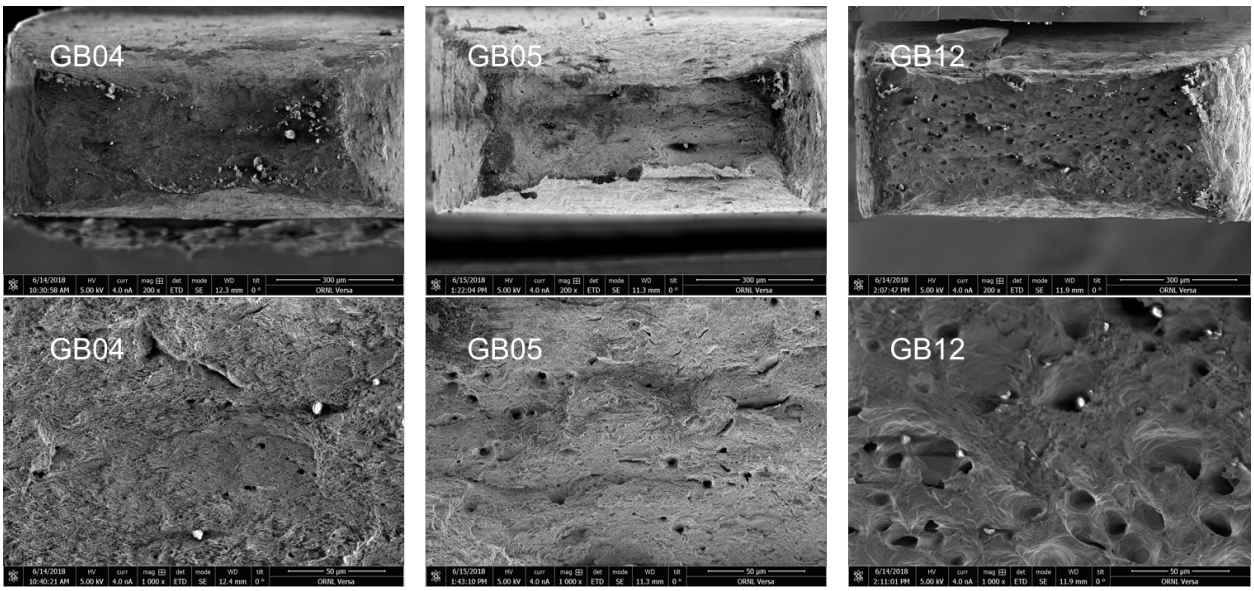

Figure 7. Fractography of the tensile-tested GB04, GB05, and GB12 samples.

5.2 IRRADIATED MICROSTRUCTURES

5.2.1 GB04 (7.44 dpa at ~490°C)

The irradiated microstructures at the tab section of the tensile-ruptured GB04 are shown in Figure 8, which is believed to be uninfluenced by the tensile stress because of the shoulder loading during the tensile test. The low-magnification bright-field (BF) scanning transmission electron microscopy (STEM) image in Figure 8a shows some precipitates, primarily at grain boundaries. The pre-existing tempered martensite seems noticeably reduced by the irradiation. Figure 8b from the large white-square-enclosed region in Figure 8a is a BF TEM image, showing two light grey $M_{23}C_6$ (M=Cr primarily) particles at a grain boundary. A dark Laves particle in a highly faulted structure is located beside one of the $M_{23}C_6$ particles. Figure 8c from the small white-square-enclosed region in Figure 8a is a high-resolution BF TEM image, showing the lattice image of the edge of the matrix precipitate. The inset of Figure 8c is a Fast Fourier

Transform (FFT) of the precipitate, which is not coherent with the matrix although it has not been indexed. Figure 8d is a BF STEM image taken from the [111] zone axis, which shows a high density of line dislocations. Radiation-induced dislocation loops are limited in this image compared to the line dislocations.

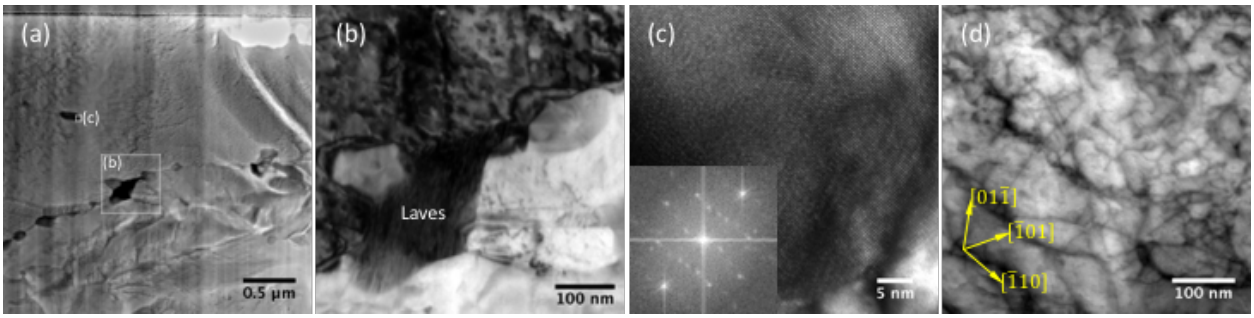

Figure 8. BF (a, d) STEM and (b-c) TEM images of GB04 showing its (a) overview, (b-c) precipitates, and (d) dislocations at the tab section of the tensile specimen.

Microstructural characterization from the gauge section and the fracture surface of GB04 was also performed. Figure 9a shows a BF STEM image from the gauge section with primarily $M_{23}C_6$ precipitates, together with some Laves particles, decorating grain boundaries. Lath structures with dislocations are seeable in Figure 9a. A matrix VN precipitate in a size of ~100 nm is shown in a BF STEM image Figure 9b, together with its selected area diffraction pattern as an inset. The weak reflections with some satellite reflections from the VN particle is partially coherent with the matrix (body-centered cubic – bcc) phase, which is identified as $[1\bar{2}0]_{VN} \parallel [1\bar{1}1]_{bcc}$ and $(422)_{VN} \parallel (011)_{bcc}$. The VN particle is interacting with a high-density of tangled dislocations, suggesting its pinning effect under tensile test. Figure 9c shows a BF STEM image from the fracture surface of GB04. Many dislocation-compiled polygonal cells in a size of ~0.4 µm formed in this region, which was resulted from the high stress in the necking zone.

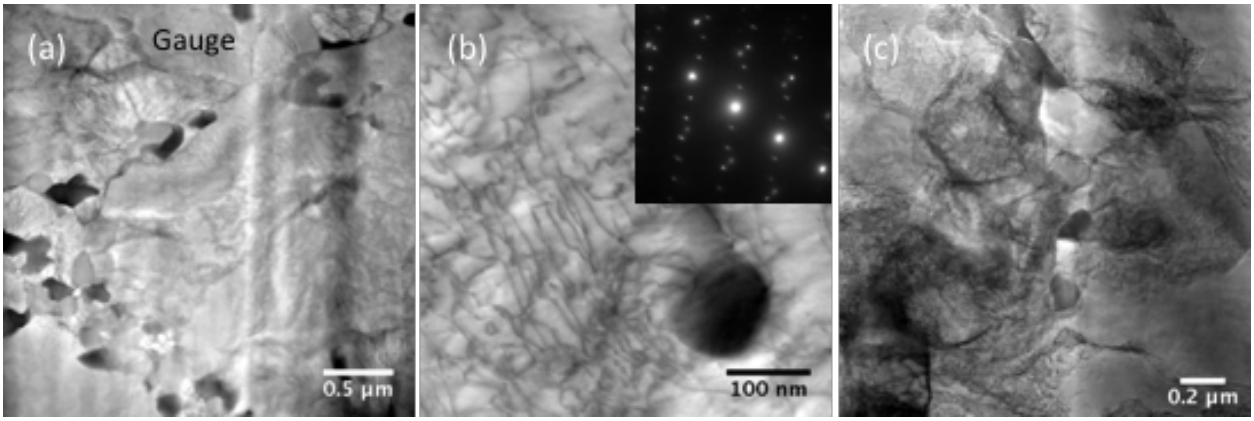

Figure 9. BF STEM images of GB04 at the (a-b) gauge and (c) fracture surface.

5.2.2 GB05 (14.66 dpa at 496.7°C)

The tab section microstructures of GB05 is shown in Figure 10, with an overview BF STEM image shown in Figure 10a, illustrating the presence of lath structures and dislocations. The high magnification BF STEM image in Figure 10b was taken from the [100] zone axis, which shows a high-density of line dislocations with limited dislocation loops. The BF TEM image in Figure 10c was taken from the lower part of Figure 10a, which shows four precipitates, labelled as p1 and p3–p5, decorating the lath boundaries and one precipitate, labelled as p2, in matrix. The high-resolution BF TEM images in Figure 10d-e exhibit examples

of the precipitates p1 and p2, respectively, from Figure 10c. Their corresponding FFTs as shown in Figure 10d-e indicate p1 and p2 as $Cr_{23}C_6$ and VN type precipitates with lattice parameters of 1.057 and 0.431 nm, respectively. The $Cr_{23}C_6$ (p1) is coherent with the matrix (m1) on the right side of p1, i.e., $[110]_{Cr_{23}C_6} \parallel [100]_{bcc}$ and $(1\bar{1}1)_{Cr_{23}C_6} \parallel (011)_{bcc}$. while the VN (p2) is fully coherent with the matrix (m1) with both of them in the [100] zone axis.

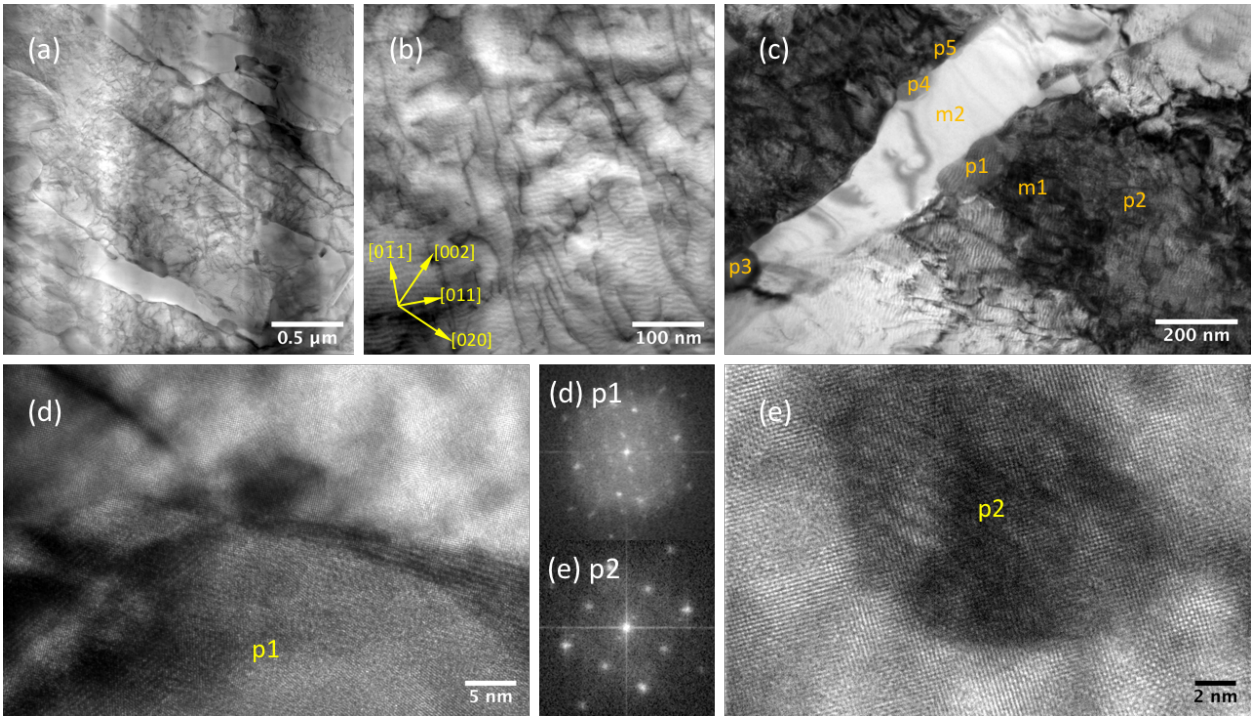

Figure 10. BF (a-b) STEM and (c-e) images and corresponding FFTs of (d-e) of GB05 at the tab section.

The BF STEM image of GB05 in the gauge section is shown in Figure 11a, with the left and lower part of the image on or close to a {111} zone axis, showing lath structures and dislocations. The upper-right side domain does not show lath structures, which is likely because it is off the zone-axis. Similar to GB04, tangled dislocations also developed in GB05 as shown in Figure 11b, with a precipitate, labelled as p, pinning dislocations. High-resolution BF TEM image of the precipitate (p) is shown in Figure 11c. The FFT inset of Figure 11c indicates good coherency with the matrix in the [111] zone axis, similar to that in the [100] zone axis as shown in Figure 10e.

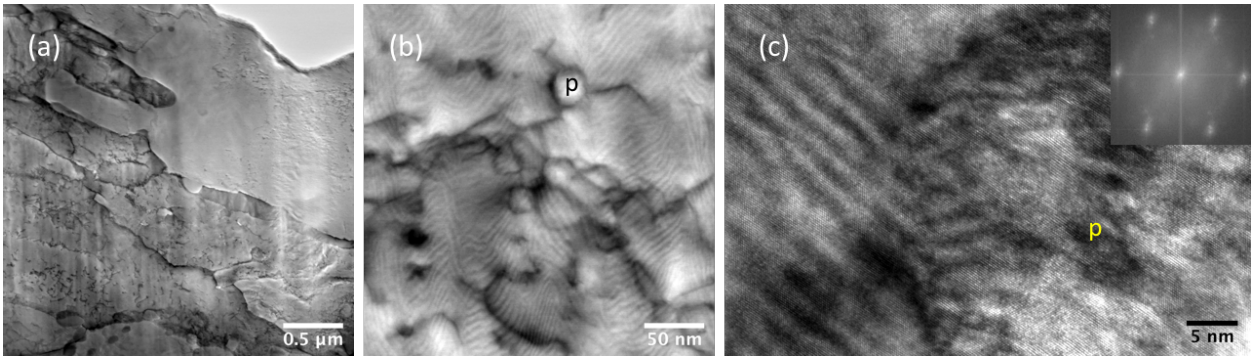

Figure 11. BF (a-b) STEM and (c) TEM images of GB05 at the gauge section.

5.2.3 GB12 (14.63 dpa at ~720°C)

Figure 12 shows the tab section microstructure of GB12. Lath structures were mostly diminished in the overview BF STEM image in Figure 12a. The higher magnification BF STEM image in Figure 12b was taken from the region near the top of Figure 12a, which exhibits a dense short dislocation sections in the [100] zone axis. Some bright spherical features were observed under BF STEM imaging condition, which is exemplified in Figure 12c. The high-resolution STEM image of one of the bright features is shown in Figure 12d, illustrating amorphous center and crystalline interface with the matrix. The FFT of the image (not shown here) indicates a singular set of bcc structure, the same as the matrix, with a diffused center suggesting the presence of amorphous from the center of the spherical center. Lattice parameter analyses from the FFTs of multiple locations in the matrix away from the bright spherical features yielded 0.3224 ± 0.0068 nm, which is relaxed to the general Fe-bcc lattice parameter of 0.2862 ± 0.0045 nm at the regions adjacent to the bright amorphized spherical features.

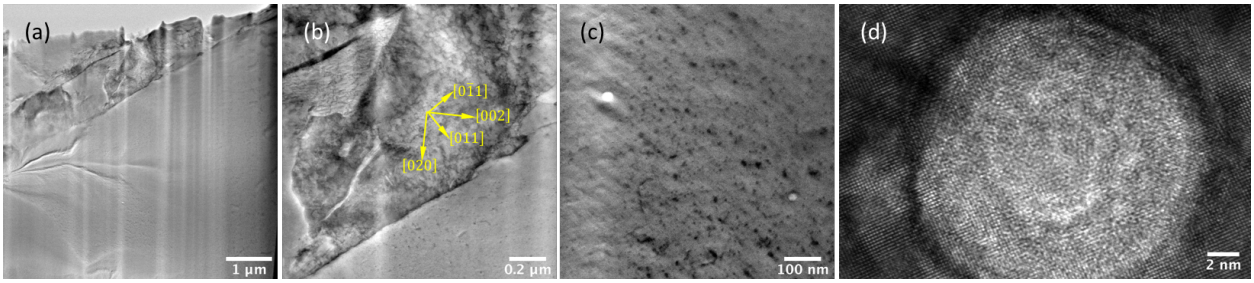

Figure 12. BF (a-b) STEM and (c-e) images and corresponding FFTs of (d-e) of GB12 at the tab section.

The microstructures of GB12 at the gauge section and the fracture surface are shown in Figure 13a-c and d, respectively. The BF STEM images of the gauge section in Figure 13a-b exhibit primarily prior-austenite grain boundaries with some partially retained lath structures, populated with dense short dislocation sections. Only a few sub-micrometer "particles", e.g., the one in Figure 13a below the "p" label, were observed in GB12. The high-resolution BF TEM of the particle-p, together with its FFT as the inset in Figure 13c, suggests that the particle-p is a ferrite domain/grain with a lattice parameter of 0.2908 nm. The microstructure at the fracture surface, where experienced the highest stress during the tensile test at room temperature, shows pronounced lath structures in Figure 13d.

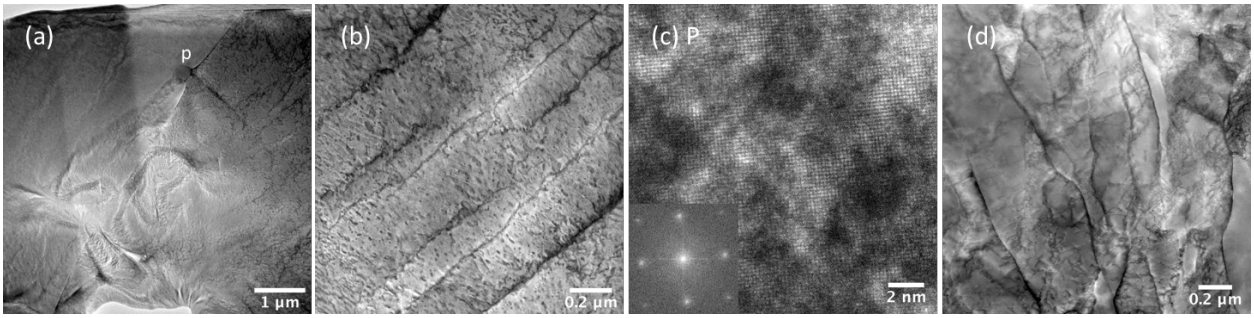

Figure 13. BF STEM images of GB12 at the (a-b) gauge and (c) fracture surface.

6. SUMMARY

Ferritic-martensitic steel Grade 92, with T91 as a reference, together with austenitic stainless steel (or Incoloy Alloy) 800H and its GBE-treated version 800H-TMP, is investigated in this project. A total of fifteen Grade 92 samples, four T91 samples, six 800H and six 800H-TMP samples were selected, which were primarily irradiated in the ATR, some in the HFIR, and few in the BOR-60 and Phénix reactors. The selected samples of Grade 92 were from two or three heats, T91 from two heats, and 800H and 800H-TMP from one heat. All the INL and ORNL samples and part of the LANL samples have been received at the IMET hot cell facility.

Tensile tests of the ORNL samples, including six Grade 92 and two 800H samples, were completed in the IMET hot cell. The Grade 92 is an optimized heat and named as G92-2b, which were irradiated in the HFIR to 0.46–14.66 dpa at 400 to ~720°C. The two 800H samples have one sample as the standard solution-annealed condition and the other sample as a TMP condition with a maximized fraction of low-Σ CSL boundaries, which were irradiated in the HFIR to 1.28 dpa at 580°C. The G92-2b samples were tested at room temperature. The lower temperature irradiation at 400–496.7°C to 0.52–14.66 dpa resulted in slight hardening or softening without noticeable changes in uniform and total plastic elongation. In contrast, the higher temperature irradiation at ~683.3–720°C to 0.46–14.63 dpa tended to reduce yield and tensile strength by about –136 to –311 MPa and plastic elongation by –1 to –3% with the increasing dose. The 800H and 800H-TMP samples were tensile-tested at their irradiation temperature 580°C, which showed >40% increase in yield and tensile strength with nearly 9% reduction in elongation for 800H-TMP compared with 800H.

Three of the selected ORNL G92-2b samples, i.e., GB04 (7.44 dpa at ~490°C), GB05 (14.66 dpa at 496.7°C), and GB12 (14.63 dpa at ~720°C), were examined at LAMDA. Vickers hardness was successfully measured on GB12, which was reduced by – (112.4 ± 12.3) HV1 from the control sample. However, the Vickers hardness measurements were failed on GB04 and GB05 because the samples were polished too thin to prevent the interference from the substrate (epoxy). The other half of the GB04 and GB05 will be polished for the hardness measurements, as well as nanoindentation studies.

Fractography of GB04, GB05, and GB12 by SEM indicated increased ductile dimples (or voids) primarily in number density with the increasing irradiation dose, while significantly increased dimples in both density and size with the increasing irradiation temperature. Microstructural characterization by TEM exhibited the presence of $Cr_{23}C_6$, VN, and Laves precipitates at boundaries and matrix, which showed pronounced precipitate-dislocation interactions (pinning effect). Dense dislocations but limited radiation-induced dislocation loops were observed in the samples, which noticeably reduced in the higher-temperature-irradiated GB12. Additionally, some tiny partially amorphized spherical domains were observed in GB12, which had a normal bcc lattice parameter of 9Cr steels at the surround regions but ~11% smaller than the lattice parameter of the matrix away from the amorphized spherical domains. Further characterization will be pursued to clarify the new findings.

REFERENCE

[1] H.J. MacLean, K. Sridharan, T.A. Hyde, Irradiation Test Plan for the ATR National Scientific User Facility – University of Wisconsin Pilot Project, INL/EXT-09-15627, June 2008.

[2] L. Tan, T.R. Allen, An electron backscattered diffraction study of grain boundary-engineered Incoloy alloy 800H, Metall. Mater. Trans. A 36 (2005) 1921–1925.

[3] L. Tan, T.R. Allen, J.T. Busby, Grain boundary engineering for structure materials of nuclear reactors, J. Nucl. Mater. 441 (2013) 661–666.

[4] L. Tan, L. Rakotojaona, T.R. Allen, R.K. Nanstad, J.T. Busby, Microstructure optimization of austenitic alloy 800H (Fe–21Cr–32Ni), Mater. Sci. Eng. A 528 (2011) 2755–2761.

[5] L. Tan, K. Sridharan, T.R. Allen, The effect of grain boundary engineering on the oxidation behavior of Incoloy alloy 800H, J. Nucl. Mater. 348 (2006) 263–271.

[6] L. Tan, K. Sridharan, T.R. Allen, Altering corrosion response via grain boundary engineering, Mater. Sci. Forum 595–598 (2008) 409–418.

[7] L. Tan, K. Sridharan, T.R. Allen, R.K. Nanstad, D.A. McClintock, Microstructure tailoring for property improvements by grain boundary engineering, J. Nucl. Mater. 374 (2008) 270–280.

[8] L. Tan, T.R. Allen, Y. Yang, Corrosion behavior of alloy 800H (Fe–21Cr–32Ni) in supercritical water, Corros. Sci. 53 (2011) 703–711.

[9] R.K. Nanstad, D.A. McClintock, D.T. Hoelzer, L. Tan, T.R. Allen, High temperature irradiation effects in selected Generation IV structural alloys, J. Nucl. Mater. 392 (2009) 331–340.

[10] L. Tan, J.T. Busby, H.J.M. Chichester, K. Sridharan, T.R. Allen, Thermomechanical treatment for improved neutron irradiation resistance of austenitic alloy (Fe–21Cr–32Ni), J. Nucl. Mater. 437 (2013) 70–74.

[11] K.L. Davis, B.M. Chase, T.C. Unruh, D.L. Knudson, J.L. Rempe, Evaluations of University of Wisconsin Silicon Carbide Temperature Monitors 300 LO and 400 LO B, INL/EXT-11-24226, December 2011.

[12] S. Wilson, et al., As-Run Thermal Analysis for the University of Wisconsin Experiment, Engineering Calculations and Analysis Report No. 3186, March 15, 2016.

[13] J. Brookman, et al., As-Run Physics Analysis for the University of Wisconsin Experiment in the ATR, Engineering Calculations and Analysis Report No. 3152, February 15, 2016.

[14] S.A. Maloy, T.A. Saleh, O. Anderoglu, T.J. Romero, G.R. Odette, T. Yamamoto, S. Li, J.I. Cole, R. Fielding, Characterization and comparative analysis of the tensile properties of five tempered martensitic steels and an oxide dispersion strengthened ferritic alloy irradiated at ≈295°C to ≈6.5 dpa, J. Nucl. Mater. 468 (2016) 232–239.

[15] L. Tan, P.J. Maziasz, T.-L. Sham, Report on the optimization and testing results of advanced ferritic/martensitic alloys, ORNL/TM-2012/288, September 14, 2012.

[16] A. Raftery, L. Tan, H. Sakasegawa, K. Linton, Tensile testing of irradiated Grade 92 ferritic-martensitic steels at the IMET hot cell facility, ORNL/LTR-2018/499, April 2018.

[17] R.K. Nanstad, D.A. McClintock, D.T. Hoelzer, L. Tan, T.R. Allen, High temperature irradiation effects in selected Generation IV structural alloys, J. Nucl. Mater. 392 (2009) 331–340.